

## Collective structures in doubly odd $^{120}\text{I}$

H. Kaur,<sup>1</sup> J. Singh,<sup>1</sup> A. Sharma,<sup>1</sup> J. Goswamy,<sup>1</sup> D. Mehta,<sup>2</sup> N. Singh,<sup>1</sup> P. N. Trehan,<sup>1</sup> E. S. Paul,<sup>3</sup> and R. K. Bhowmik<sup>4</sup>

<sup>1</sup>Department of Physics, Panjab University, Chandigarh-160014, India

<sup>2</sup>Department of Physics and Astrophysics, University of Delhi, Delhi-110007, India

<sup>3</sup>Oliver Lodge Laboratory, University of Liverpool, P.O. Box 147, Liverpool L69 3BX, United Kingdom

<sup>4</sup>Nuclear Science Centre, Jawahar Lal Nehru University, New Delhi-110067, India

(Received 14 August 1996)

High spin states in the doubly odd  $^{120}\text{I}$  nucleus have been investigated through in-beam gamma-ray spectroscopy following the  $^{108}\text{Pd}+^{16}\text{O}$  and  $^{114}\text{Cd}+^{11}\text{B}$  fusion-evaporation reactions. A new  $\Delta I=1$  collective band, based on the  $\pi g_{7/2} \otimes \nu h_{11/2}$  quasiparticle configuration, has been identified. This band exhibits energy staggering in the odd-even spin states and is found to be intense as compared to the earlier known  $\pi g_{9/2}^{-1} \otimes \nu h_{11/2}$  nonstaggered band. A loss in collectivity is observed at the  $I^\pi=(23^-)$  state, implying an abrupt band termination. [S0556-2813(97)03701-1]

PACS number(s): 21.10.Re, 23.20.Lv, 21.60.-n, 27.60.+j

Recent  $\gamma$ -ray spectroscopic investigations have revealed a variety of nuclear shapes in the odd- $A$   $^{113-121}\text{I}$  nuclei [1-5]. In these nuclei, the yrast collective prolate band based on the low- $\Omega$   $\pi h_{11/2}[550]1/2^-$  intruder [1-5] as well as the collective oblate ( $\gamma=-60^\circ$ )  $\Delta I=1$  band, based on the high- $\Omega$   $\pi h_{11/2}[505]11/2^-$  orbital [4,5], have been identified. Also, the particle-hole configurations involving the  $\pi g_{9/2}[404]9/2^+$  extruder, which is responsible for inducing quadrupole deformation and hence collective bands in the spherical Sn [6] and Sb [7] nuclei, persist in the I nuclei [1-5]. Further, the collective oblate and prolate single-quasiparticle bands, based on the  $\pi g_{7/2}(d_{5/2})$  orbitals, have been identified in the odd- $A$   $^{117-121}\text{I}$  nuclei [4,5]. The yrast  $\pi h_{11/2}$  band in  $^{115-121}\text{I}$  [2,4,5] is terminated with the abrupt appearance of a favored noncollective oblate state at  $I \sim 21\hbar$  while, in the lighter  $^{113,115}\text{I}$  nuclei [1,3], newly discovered intruder bands show the unique feature of smooth termination. In view of the wide variety of structural features observed in the odd- $A$  iodine nuclei, it is of recent interest to probe analogous bands, based on the above-mentioned active proton orbitals coupled to the odd neutron in  $h_{11/2}$ ,  $g_{7/2}$ , or  $d_{5/2}$  orbitals, in the doubly odd neighbors. Previous information on the doubly odd  $^{116-122}\text{I}$  nuclei [8] was limited to the  $\Delta I=1$  collective band associated with the coupling of the  $h_{11/2}$  neutron to the  $g_{9/2}[404]9/2^+$  proton-hole orbital. The study of collective structures in the doubly odd iodine nuclei has recently enjoyed upsurge in activity and investigations have revealed collective bands based on  $\pi g_{7/2} \otimes \nu h_{11/2}$  in  $^{112,114,118}\text{I}$  [9-12],  $\pi g_{9/2}^{-1} \otimes \nu h_{11/2}$  in  $^{114}\text{I}$  [10], and  $\pi h_{11/2} \otimes \nu h_{11/2}$  in  $^{116,118}\text{I}$  [13,12]. In the case of  $^{116}\text{I}$  [14], a  $(23^-)$  state has been interpreted in terms of an yrast noncollective oblate ( $\gamma=+60^\circ$ ) state. This paper presents the results on the doubly odd  $^{120}\text{I}$  nucleus, investigated through in-beam  $\gamma$ -ray spectroscopy following the fusion-evaporation reactions.

The high spin states in  $^{120}\text{I}$  were populated through  $^{108}\text{Pd}+^{16}\text{O}$  and  $^{114}\text{Cd}+^{11}\text{B}$  fusion-evaporation reactions at 84 and 60 MeV, respectively. The heavy-ion projectiles were delivered by the 15UD Pelletron accelerator at the Nuclear Science Centre (NSC), New Delhi. Isotopically enriched foils of  $^{108}\text{Pd}$  ( $\sim 1 \text{ mg/cm}^2$ ) and  $^{114}\text{Cd}$  ( $\sim 3 \text{ mg/cm}^2$ ) rolled on

thick Pb backing were used as targets. The emitted  $\gamma$  rays were recorded using the Gamma Detector Array (GDA) setup consisting of 8 Compton-suppressed Ge detectors and a 14-element BGO (bismuth germanate) multiplicity filter. The Ge detectors were mounted in two groups making angles of  $99^\circ$  and  $153^\circ$  with the beam direction and tilted at  $\pm 23^\circ$  with respect to the horizontal plane. The multiplicity filter consisted of two sets of seven closely packed hexagonal BGO elements mounted above and below the target chamber. A coincidence resolving time  $2\tau=200$  ns was used to collect  $\gamma$ - $\gamma$  coincidences. A total of 75 and 100 million Ge-Ge-BGO coincidences were recorded for the  $^{108}\text{Pd}+^{16}\text{O}$  and  $^{114}\text{Cd}+^{11}\text{B}$  reactions, respectively. The coincidence data were sorted, event by event, into two-dimensional  $E_\gamma-E_\gamma$  matrix and background-subtracted coincidence spectra were generated for further analysis. The level scheme of  $^{120}\text{I}$  deduced from the present work, shown in Fig. 1, depicts two coupled bands (labeled 1 and 3) and a sequence of  $E2$  transitions (labeled 2). Details regarding the assignment of the new bands to  $^{120}\text{I}$  on the basis of cross-bombardment results have been given elsewhere [15]. The placement of  $\gamma$  transitions in the level scheme is based on their intensities, energy sums, and coincidence relationships. In order to obtain information on the  $\gamma$  ray multiplicities, directional correlation (DCO) ratios [ $R_{\text{DCO}}=I_\gamma(153^\circ)/I_\gamma(99^\circ)$ ] were determined. The coincidence events were sorted into an asymmetric matrix with  $153^\circ$  detectors on one axis and  $99^\circ$  detectors on the other axis, which was used to obtain  $R_{\text{DCO}}$ . Further,  $M1$  multipolarity could be assigned to some of the low energy dipole transitions by balancing the intensity flow (corrected for internal conversion) as seen in the coincidence spectra obtained by gating the higher lying transitions in the total  $E_\gamma-E_\gamma$  matrix. The energies, intensities, DCO ratios and the assigned multiplicities for transitions in  $^{120}\text{I}$  from the  $^{114}\text{Cd}+^{11}\text{B}$  reaction, along with their placements in the level scheme are given in Table I.

The spin-parity to the ground state ( $T_{1/2}=81$  m) of  $^{120}\text{I}$  had been assigned as  $I^\pi=(2^-)$  from the radioactive  $\beta^+$  decay studies of  $^{120}\text{Xe}$  [16]. An excited isomeric state ( $T_{1/2}=53$  m) with  $I^\pi=(7^-)$  had also been identified but its placement with respect to the ground state is not known.

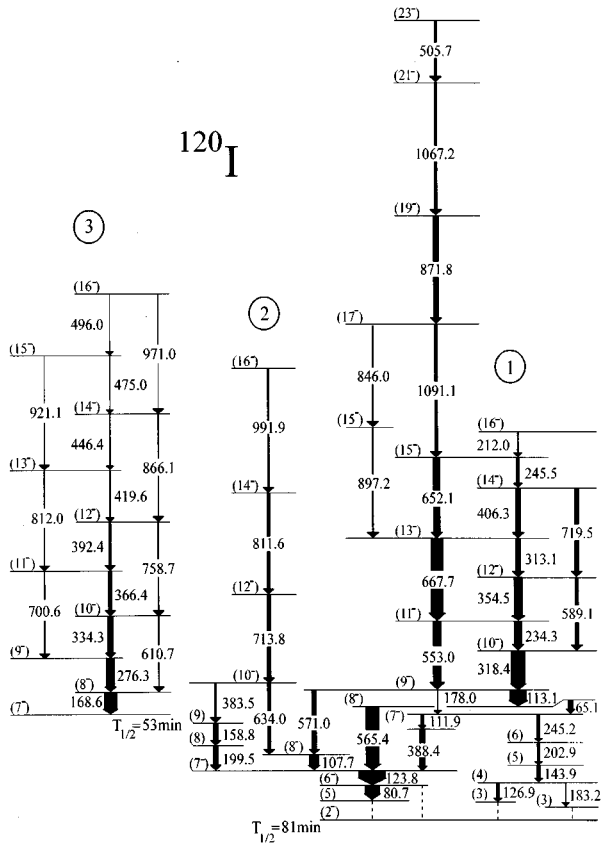


FIG. 1. Level scheme of  $^{120}\text{I}$  deduced from the present work.

Previous investigations on the high spin states in  $^{120}\text{I}$ , by Quader *et al.* [8], revealed a  $\Delta I=1$  collective band decaying onto the  $I^\pi=(7^-)$  isomeric state. The present work has extended this band (labeled 3 in Fig. 1) to  $I^\pi=(16^-)$  by the addition of the 475 and 496 keV dipole transitions and the 921 and 971 keV quadrupole crossovers. The low spin structure, below bands 1 and 2, consists of several parallel decay paths and low energy (highly converted) transitions are ex-

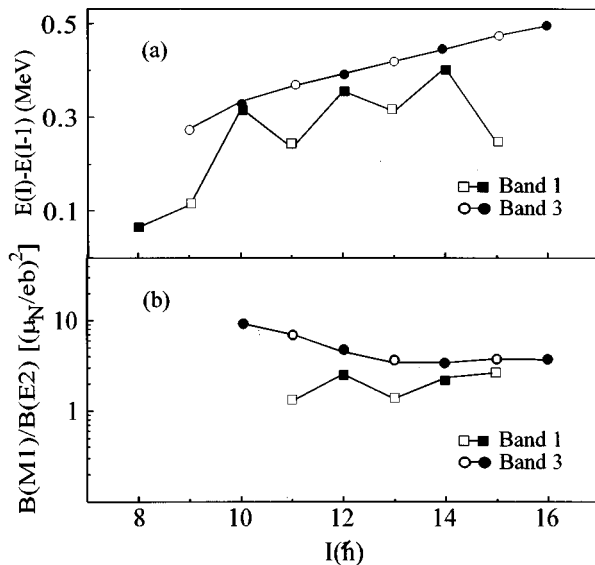


FIG. 2. Plot of (a)  $E(I) - E(I-1)$  and (b)  $B(M1)/B(E2)$  values vs spin for bands 1 and 3.

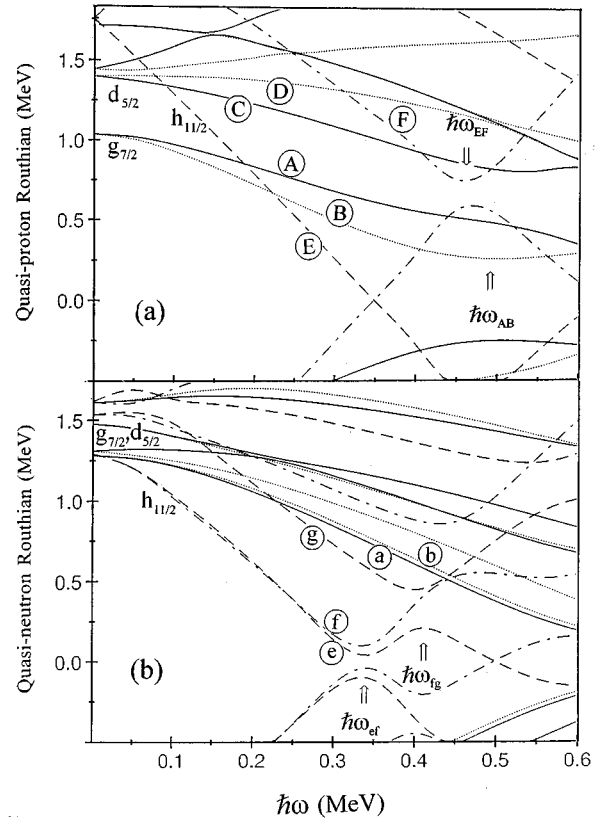


FIG. 3. Cranked Woods-Saxon Routhians for (a) protons and (b) neutrons in  $^{120}\text{I}$ . The parity and signature  $(\pi, \alpha)$  of the levels are  $(+, +1/2)$ , solid line;  $(+, -1/2)$ , dotted lines;  $(-, -1/2)$ , dashed line;  $(-, +1/2)$ , dot-dashed lines.

pected to complete the decay to the  $(2^-)$  ground state (Fig. 1).

The coupled band 1 is characterized by intense  $E2$  cross-over transitions in the odd-spin signature partner compared to those in the even-spin signature partner. A plot of level-energy differences  $[E(I) - E(I-1)]$  as a function of spin [Fig. 2(a)] reveals energy staggering in the odd-even spin states in this band. The experimental  $B(M1)/B(E2)$  values also show a signature dependence and average to  $\sim 2(\mu_N/eb)^2$  [Fig. 2(b)]. This band shows a small signature splitting,  $\Delta e' \approx 60$  keV, with the Routhian for the odd-spin ( $\alpha=1$ , favored) partner lying lower than the even-spin ( $\alpha=0$ ,

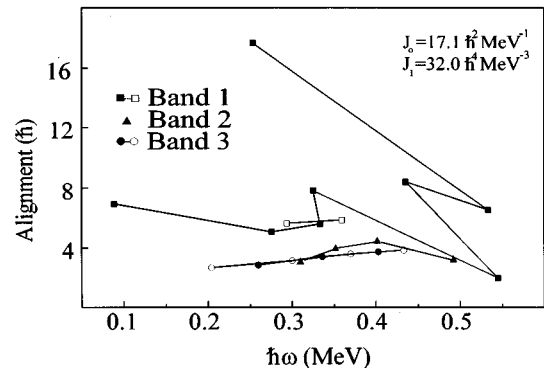


FIG. 4. Experimental alignment plots for bands 1-3.

TABLE I. Properties of the transitions assigned to  $^{120}\text{I}$ .

| $E_\gamma(\text{keV})^a$ | $I_\gamma^b$    | $R_{\text{DCO}}$      | Multipolarity | Placement                   | $E_\gamma(\text{keV})^a$ | $I_\gamma^b$ | $R_{\text{DCO}}$ | Multipolarity | Placement                   |
|--------------------------|-----------------|-----------------------|---------------|-----------------------------|--------------------------|--------------|------------------|---------------|-----------------------------|
| 65.1                     | 20              | 0.70 (15)             | $M1$          | $(8^-) \rightarrow (7^-)$   | 419.6                    | 5            | 0.42 (14)        | $M1$          | $(13^-) \rightarrow (12^-)$ |
| 80.7                     | 55              | 0.71 (8)              | Dipole        | $(6^-) \rightarrow (5^-)$   | 446.4                    | 4            | 0.57 (12)        | $M1$          | $(14^-) \rightarrow (13^-)$ |
| 107.7                    | 35              | 0.68 (9)              | $(M1)$        | $(8^-) \rightarrow (7^-)$   | 475.0                    | 2            | 0.61 (15)        | $M1$          | $(15^-) \rightarrow (14^-)$ |
| 111.9                    | 12              | c                     | Dipole        | Below $(7^-)$               | 496.0                    | 2            |                  | $(M1)$        | $(16^-) \rightarrow (15^-)$ |
| 113.1                    | 62              | 0.62 (8) <sup>c</sup> | $M1$          | $(9^-) \rightarrow (8^-)$   | 505.7                    | 9            | 1.09 (17)        | $E2$          | $(23^-) \rightarrow (21^-)$ |
| 123.8                    | 100             | 0.66 (7)              | $M1$          | $(7^-) \rightarrow (6^-)$   | 553.0                    | 63           | 1.17 (12)        | $E2$          | $(11^-) \rightarrow (9^-)$  |
| 126.9                    | 13              | 0.50 (8)              | Dipole        | $(4^-) \rightarrow (3^-)$   | 565.4                    | 49           | 0.65 (8)         | $M1$          | $(8^-) \rightarrow (7^-)$   |
| 143.9                    | 16              | 0.39 (8)              | Dipole        | $(5^-) \rightarrow (4^-)$   | 571.0                    | 19           | 0.52 (7)         | $M1$          | $(9^-) \rightarrow (8^-)$   |
| 158.8 <sup>c,d</sup>     | 32 <sup>c</sup> | 0.64 (9) <sup>c</sup> | Dipole        | $(9^-) \rightarrow (8^-)$   | 589.1                    | 14           | 1.5 (3)          | $E2$          | $(12^-) \rightarrow (10^-)$ |
| 168.6                    | 49              | 0.47 (6)              | $M1$          | $(8^-) \rightarrow (7^-)$   | 610.7                    | 4            |                  | $E2$          | $(10^-) \rightarrow (8^-)$  |
| 178.0                    | 6               |                       | $E2$          | $(9^-) \rightarrow (7^-)$   | 634.0                    | 14           | 1.03 (15)        | $E2$          | $(10^-) \rightarrow (8^-)$  |
| 183.2                    | 4               | 0.51 (9)              | Dipole        | $(4^-) \rightarrow (3^-)$   | 652.1                    | 26           | 1.14 (12)        | $E2$          | $(15^-) \rightarrow (13^-)$ |
| 199.5                    | 21              | 0.69 (10)             | Dipole        | $(8^-) \rightarrow (7^-)$   | 667.7                    | 46           | 1.08 (10)        | $E2$          | $(13^-) \rightarrow (11^-)$ |
| 202.9                    | 13              | 0.57 (9)              | Dipole        | $(6^-) \rightarrow (5^-)$   | 700.6                    | 5            | 1.03 (12)        | $E2$          | $(11^-) \rightarrow (9^-)$  |
| 212.0                    | 9               |                       | $(M1)$        | $(16^-) \rightarrow (15^-)$ | 713.8                    | 16           | 1.05 (16)        | $E2$          | $(12^-) \rightarrow (10^-)$ |
| 234.3                    | 29              | 0.65 (7)              | $M1$          | $(11^-) \rightarrow (10^-)$ | 719.5                    | 18           | 0.96 (14)        | $E2$          | $(14^-) \rightarrow (12^-)$ |
| 245.2                    | 12              | c                     | Dipole        | $(7^-) \rightarrow (6^-)$   | 758.7                    | 5            | 0.97 (14)        | $E2$          | $(12^-) \rightarrow (10^-)$ |
| 245.5                    | 13              | 0.66 (9) <sup>c</sup> | $M1$          | $(15^-) \rightarrow (14^-)$ | 811.6                    | 13           | 1.14 (19)        | $E2$          | $(14^-) \rightarrow (12^-)$ |
| 276.3                    | 32              | 0.49 (7)              | $M1$          | $(9^-) \rightarrow (8^-)$   | 812.0                    | 5            | 0.82 (18)        | $E2$          | $(13^-) \rightarrow (11^-)$ |
| 313.1                    | 21              | 0.63 (7)              | $M1$          | $(13^-) \rightarrow (12^-)$ | 846.0                    | 6            | 0.88 (20)        | $E2$          | $(17^-) \rightarrow (15^-)$ |
| 318.4                    | 54              | 0.58 (5)              | $M1$          | $(10^-) \rightarrow (9^-)$  | 866.1                    | 4            | 1.02 (17)        | $E2$          | $(14^-) \rightarrow (12^-)$ |
| 334.3                    | 22              | 0.53 (7)              | $M1$          | $(10^-) \rightarrow (9^-)$  | 871.8                    | 20           | 1.08 (14)        | $E2$          | $(19^-) \rightarrow (17^-)$ |
| 354.5                    | 32              | 0.51 (6)              | $M1$          | $(12^-) \rightarrow (11^-)$ | 897.2                    | 6            | 0.99 (19)        | $E2$          | $(15^-) \rightarrow (13^-)$ |
| 366.4                    | 14              | 0.51 (8)              | $M1$          | $(11^-) \rightarrow (10^-)$ | 921.1                    | 2            |                  | $E2$          | $(15^-) \rightarrow (13^-)$ |
| 383.5                    | 7               | 0.38 (9)              | Dipole        | $(10^-) \rightarrow (9^-)$  | 971.0                    | 2            |                  | $(E2)$        | $(16^-) \rightarrow (14^-)$ |
| 388.4                    | 22              | 0.60 (6)              | Dipole        | Feeding $(7^-)$             | 991.9                    | 8            | 0.95 (20)        | $E2$          | $(16^-) \rightarrow (14^-)$ |
| 392.4                    | 8               | 0.52 (8)              | $M1$          | $(12^-) \rightarrow (11^-)$ | 1067.2                   | 11           | 1.10 (20)        | $E2$          | $(21^-) \rightarrow (19^-)$ |
| 406.3                    | 20              | 0.59 (7)              | $M1$          | $(14^-) \rightarrow (13^-)$ | 1091.1                   | 12           | 1.02 (18)        | $E2$          | $(17^-) \rightarrow (15^-)$ |

<sup>a</sup>Accurate to 0.3 keV.

<sup>b</sup>Errors in  $\gamma$ -ray intensities are 10–20 %.

<sup>c</sup>Value given for the doublet transitions.

<sup>d</sup>Another transition of similar energy is observed in the decay from the  $(5^-)$  state.

unfavored) partner. This indicates that either or both of the proton and neutron orbitals, involved in the configuration of band 1, have small signature splitting. The  $\pi h_{11/2}(\Omega=1/2)$ ,  $\pi g_{7/2}(\Omega=3/2)$ , and  $\pi d_{5/2}(\Omega=1/2)$  orbitals near the proton Fermi surface exhibit large signature splitting [Fig. 3(a)]. The  $\nu h_{11/2}(\Omega=5/2)$  orbital with nearly degenerate signatures [Fig. 3(b)], is therefore likely to be the neutron partner in the configuration of this band. Further the possibility of  $\pi h_{11/2}$  as proton partner is ruled out as the  $\pi h_{11/2} \otimes \nu h_{11/2}$  bands in the neighboring doubly odd  $^{116,118}\text{I}$  isotopes [13,12] show alignment value,  $\sim 8\hbar$ , larger than that observed for this band (Fig. 4). This band is therefore assigned the  $\pi g_{7/2} \otimes \nu h_{11/2}$  configuration. A staggered band based on the same configuration has also been observed in the lighter  $^{114}\text{I}$  isotopes [10], with large signature splitting ( $\Delta e' \approx 300$  keV) and in  $^{118}\text{I}$  [11,12], with small signature splitting ( $\Delta e' \approx 30$  keV). The two signatures of the  $h_{11/2}$  neutron orbital in  $^{114}\text{I}$ , being of low  $\Omega$ , exhibit large splitting [10] while in the heavier  $^{118}\text{I}$  [11,12] and  $^{120}\text{I}$  isotopes these are almost degenerate [Fig. 3(b)]. Calculations based on the total Routhian surface (TRS) formalism [17–19], using a universal Woods-Saxon single-particle potential, predict shape parameters  $\beta_2=0.19$ ,  $\gamma=+8^\circ$  for the  $\pi g_{7/2} \otimes \nu h_{11/2}$  configura-

tion. The decay of band 1 having not been established completely, the spin assignments have been done by comparing this band with the analogous band in the doubly odd  $^{118}\text{I}$  [12].

Woods-Saxon cranking calculations, both for protons and neutrons, have been performed at the deformation predicted by the TRS calculations [17–19]. The calculations predict the alignment of the first  $\nu h_{11/2}^2$  (**ef**) pair at  $\hbar\omega_{ef}=0.35$  MeV [Fig. 3(b)], which is blocked for the assigned  $\pi g_{7/2} \otimes \nu h_{11/2}$  (**Be**) configuration. Since the next  $\nu h_{11/2}^2$  (**fg**) pair alignment is predicted at frequency  $\hbar\omega_{fg}=0.42$  MeV [Fig. 3(b)], which is lower than that for the alignment of the  $\pi h_{11/2}^2$  (**EF**) pair [Fig. 3(a)], the favored signature of band 1 possibly progresses into the  $\pi g_{7/2} \otimes \nu(h_{11/2})^3$  configuration at higher spins. These results are somewhat difficult to harmonize with the experimental observations where no sharp alignment is evident (Fig. 4). The favored signature partner of this collective band has been established upto  $I^\pi=(23^-)$ . The presence of the low energy 506 keV [ $(23^-) \rightarrow (21^-)$ ] stretched  $E2$  transition in this band indicates loss of collectivity. The energies of the states of band 1, relative to a rotating liquid drop energy reference, are presented as a function of spin in Fig. 5. The noncollective  $(23^-)$  state is

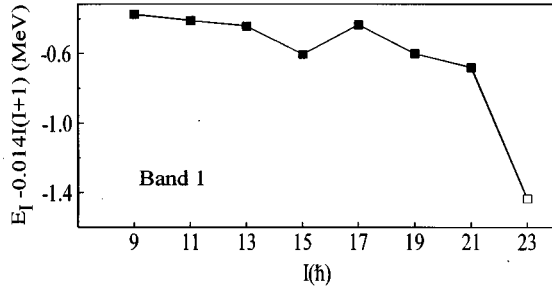


FIG. 5. Level energies relative to a rigid-rotor vs spin in the favored partner of band 1.

seen to drop to a much lower energy. Also, in spite of the good intensity of the uppermost observed 506 keV transition (Fig. 6), no further transitions could be identified, which is possibly due to fragmentation of the structure above the  $(23^-)$  state. These features suggest a possible band termination at  $I^\pi = (23^-)$ . The TRS calculations indeed predict a fully aligned noncollective oblate state ( $\gamma = +60^\circ$ ) at spin  $I^\pi = (21^-)$  with  $[\pi g_{7/2} d_{5/2}^2]_{15/2+} \otimes [\nu h_{11/2}^3]_{27/2-}$  configuration. In view of the tentative spin assignments, this predicted state may correspond to the experimentally observed noncollective state at  $I^\pi = (23^-)$ .

Band 2 is found to comprise of a sequence of stretched  $E2$  transitions. The signature partner of this band has not been observed, which indicates a possible large signature splitting. This band is proposed to be based on the  $\pi h_{11/2} \otimes \nu d_{5/2}$  configuration on the basis of additivity of alignment arguments [20]. The observed alignment for this band is  $\sim 4\hbar$  (Fig. 4) and is close to the added contributions of the proton ( $\sim 4\hbar$ ), deduced from the  $\pi h_{11/2}$  yrast band in  $^{119,121}\text{I}$  [5], and that of the neutron ( $\sim 0.5\hbar$ ), deduced from the  $\nu d_{5/2}$  band in  $^{119}\text{Xe}$  [21]. The possibility of the  $\nu h_{11/2}$  or  $\nu g_{7/2}$  as the neutron partner in the configuration is unlikely as it will lead to higher added alignment values ( $> 6\hbar$ ) [15,21]. A cascade of 477, 595, and 920 keV transitions has been observed above the  $(16^-)$  state of band 2 (not shown in Fig. 1). This cascade is also found to feed significantly to the

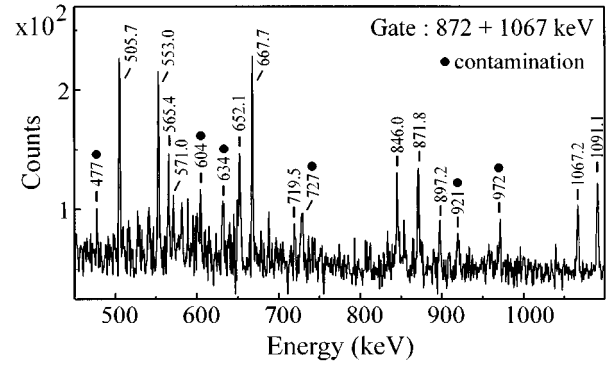


FIG. 6. Part of the added  $\gamma$  ray coincidence spectrum with gates on the 872 and 1067 keV transitions in band 1.

levels of bands 1 and 3 (Fig. 2 of [15]). However, definite links could not be ascertained. In view of the complex decay of this cascade, it is not likely to be the extension of band 2, as reported earlier [15].

The coupled band 3, consisting of intense  $\Delta I = 1$  interweaving transitions with weaker  $E2$  crossover transitions, exhibits nonstaggered behavior [Fig. 2(a)]. The measured  $B(M1)/B(E2)$  values for this band average to  $\sim 5(\mu_N/e b)^2$  [Fig. 2(b)], which are comparable to those observed for the  $\pi g_{9/2}^{-1}$  band in the neighboring  $^{117,121}\text{I}$  nuclei [4,5]. The experimental alignment plot for this band (Fig. 4) does not show any upbend up to  $\hbar\omega \sim 0.44$  MeV. The  $\nu h_{11/2}^2$  band crossing, which occurs at  $\hbar\omega = 0.39$  MeV in the  $\pi g_{9/2}^{-1}$  band in the neighboring odd-A iodine nuclei [5], is absent in this case. These facts favor the earlier assigned  $\pi g_{9/2}^{-1} \otimes \nu h_{11/2}$  configuration [8] for this band.

In summary, from the present investigations, a new coupled band (labeled 1) based on the  $\pi g_{7/2} \otimes \nu h_{11/2}$  configuration has been identified in  $^{120}\text{I}$ . A loss in collectivity is observed at  $I^\pi = (23^-)$  state, implying a possible abrupt band termination.

The authors thank the GDA staff and accelerator crew at NSC, New Delhi, for their cooperation. Financial support from UGC, CSIR, and DAE, India, and EPSRC (U.K.) is duly acknowledged.

[1] M. P. Waring *et al.*, Phys. Rev. C **51**, 2427 (1995).  
 [2] E. S. Paul *et al.*, J. Phys. G **18**, 837 (1992).  
 [3] E. S. Paul *et al.*, Phys. Rev. C **50**, 741 (1994).  
 [4] M. P. Waring *et al.*, Phys. Rev. C **48**, 2629 (1993).  
 [5] Y. Liang *et al.*, Phys. Rev. C **45**, 1041 (1992).  
 [6] R. Wadsworth *et al.*, Nucl. Phys. **A559**, 461 (1993).  
 [7] E. S. Paul *et al.*, Phys. Rev. C **50**, 2297 (1994).  
 [8] M. A. Quader *et al.*, Phys. Rev. C **30**, 1772 (1984).  
 [9] E. S. Paul *et al.*, J. Phys. G **21**, 1001 (1995).  
 [10] E. S. Paul *et al.*, Phys. Rev. C **52**, 1691 (1995).  
 [11] H. Kaur *et al.*, Z. Phys. A **350**, 183 (1994).

[12] E. S. Paul *et al.*, J. Phys. G **22**, 653 (1996).  
 [13] E. S. Paul *et al.*, J. Phys. G **21**, 995 (1995).  
 [14] E. S. Paul *et al.*, J. Phys. G **19**, 343 (1993).  
 [15] H. Kaur *et al.*, Z. Phys. A **352**, 11 (1995).  
 [16] A. Hashizume *et al.*, Nucl. Data Sheets **52**, 641 (1987).  
 [17] W. Nazarewicz *et al.*, Nucl. Phys. **A467**, 437 (1987).  
 [18] R. Wyss *et al.*, Phys. Lett. B **215**, 211 (1988).  
 [19] W. Nazarewicz *et al.*, Nucl. Phys. **A503**, 285 (1989).  
 [20] S. Drissi *et al.*, Nucl. Phys. **A451**, 313 (1986).  
 [21] V. P. Janzen *et al.*, Phys. Rev. C **39**, 2050 (1989).